Solid Freeform Fabrication 2022: Proceedings of the 33rd Annual International Solid Freeform Fabrication Symposium – An Additive Manufacturing Conference
Reviewed Paper

Effect of Build Orientation on Residual Stress and Microstructure in Inconel 625 Fabricated via Laser Powder Bed Fusion

M. Andurkar[1], B. C. Prorok[2], S. M. Thompson[*1]

[1] Alan Levin Department of Mechanical and Nuclear Engineering, Kansas State University, Manhattan, KS 66502, United States of America

[2] Department of Materials Engineering, Auburn University, Auburn, AL 36849, United States of America

*Corresponding author: smthompson@ksu.edu

Abstract

The reliability of parts produced by Laser Powder Bed Fusion (L-PBF) is still not at a great acceptance level. One of the major defects inherited in parts fabricated from L-PBF is a high level of residual stress. In this study, two build orientations i.e., vertical and diagonal, were used to fabricate Inconel 625 specimens to observe its effects on the residual stress magnitude and grain growth. A novel, Cos-α X-ray diffraction method was used to measure residual stress values along the top surface of the samples. Electron Backscattered Diffraction (EBSD) and kernel average misorientation (KAM) maps were employed to explain residual stress trends and differences between samples. Results indicate that the as-printed vertical sample possessed a higher tensile residual stress (77 ± 15 MPa) compared to the diagonally-printed sample (52 ± 12 MPa). The KAM map of the as-printed vertically oriented sample showed more pronounced local misorientations caused by dislocations compared to the diagonally-printed sample.

Keywords: Selective Laser Melting, Nickel Superalloy, EBSD, Misorientation, Microstrain

1. Introduction

The Laser powder bed fusion (L-PBF) process is one of the seven different categories of additive manufacturing (AM) technologies according to the ASTM 52900:2021 [1]. The importance and interest of this technology has proliferated in various industrial sectors, in particular aerospace, automotive, nuclear, biomedical. L-PBF offers several advantages like fabricating complex geometries, rapid design to manufacture cycles, reduction of wasted materials, and an ability to tailor properties of end-user components during the fabrication process. The L-PBF process consists of melting consecutive powder layers by a focused laser beam guided by 3D-computer aided design (CAD). The presence of support structures and the powder bed itself allows L-PBF to be capable of building complex shapes of metal parts that would be challenging to fabricate using conventional methods. Laser employed manufacturing methods involve large thermal gradients in the vicinity of the targeted region due to high heat flux. The melted layers are subsequently subjected to extremely high cooling rates (around 10^5–10^6 ºC/s) that generate large non-uniform thermal gradients. This large thermal gradients precede the formation of residual stress also known as 'hidden stress'. Residual stress left unmanaged in the finished product can lead to part distortion, delamination, parts built outside geometric tolerances, increased risk of crack formation, and reduced fatigue performance [2].

Nickel based superalloys are known to be notoriously challenging to use in machining, as wells as conventional casting or forging methods due to its high hardness, low thermal conductivity, and high work hardening rate [3], [4]. Inconel 625 (IN625) is a nickel based solid solution strengthening superalloy which derives its strengthening ability largely from the presence of molybdenum (Mo) and Niobium (Nb) elements. IN625 finds its application in different industry sectors such as aeronautics, aerospace, nuclear, chemical and petrochemical due to superior properties like high-temperature strength, high creep resistance, and corrosion resistance [5], [6][7]. Due to challenges posed by using subtractive manufacturing methods and the recent bombarding developments of AM technology, fabrication of IN625 components by AM according to industrial standards has emerged as a promising approach. However, IN625 parts produced by methods such as L-PBF still cause challenges like the formation of residual stress. A careful selection of process parameters, scan strategy, build orientation is needed to fabricate parts with optimized microstructure, density, and mechanical properties.

In the past, studies have been conducted to understand the effects of different scan strategies and build orientations on the formation of residual stress in different materials. Pant et al. mapped residual stress in Inconel 718 produced by L-PBF in three orientations (vertical, diagonal, horizontal). They observed the vertical sample inherited the highest tensile residual stress followed by the diagonal and horizontal samples [8]. Some studies reported the greatest residual stress was generated perpendicular to scan direction [9], while others have observed the greatest residual stress parallel to scan vectors [10]. In addition, unidirectional scan vectors may give rise to higher anisotropic residual stress compared to checkerboard or alternating scanning strategies since longer scanning paths introduce heterogenous thermal gradients [11]. To understand the effects of different scan strategies and build orientation on residual stress formation in AM parts, accurate and reliable residual stress measurement techniques are critical.

Measurement of residual stress can be carried out using destructive or non-destructive methods. Non-destructive testing (NDT) category involves X-ray, neutrons, synchrotron radiation, and magnetic strain[12]. X-ray diffraction (XRD) is one of the most matured technologies among all NDT methods. XRD is used to measure residual stress on external surface and sub-surface with high accuracy. XRD typically relies on using the $\sin^2\Psi$ method for calculating stresses. The XRD-$\sin^2\Psi$ stress method begins with XRD scans along series of defined incident angles (Ψ) over a pre-determined diffraction angle. From the scans performed at each incident angle, the selected diffraction peak position must be accurately verified, i.e., the 2θ value must be measured from a very wide-ranging and sometimes unevenly shaped peak. The obtained 2θ values are then used to execute the linear regression to obtain the slope and intercept values to be used for the stress calculation. Line detectors are usually used in the $\sin^2\Psi$ method which captures a small part of the Debye-Scherrer (D-S) ring at every incident angle (Ψ). The D-S ring is created by a diffraction pattern occurring due to Braggs law when X-rays are incident on a polycrystalline material. To eliminate the extensive process time to obtain data from this method, a novel method of Cos α was developed in 1978. The Cos α method employs the entire D-S ring produced from single exposure of X-rays at a single incident X-ray beam angle captured by a 2-D detector. The Cos α method has several advantages over the traditional $\sin^2\Psi$ method such as simple optical setup and faster in-plane normal and shear stress calculations [13]. The accuracy of this novel method was tested against the traditional $\sin^2\Psi$ method and it was found to provide reliable results.

In this current work, the effect of build orientation i.e., vertical and diagonal on residual stress value and grain morphology in Inconel 625 produced by laser powder bed fusion additive

manufacturing process. A novel method was used to measure residual stress which is proven to be easier, quicker, and reliable. A comparison of residual stress between two build orientations was discussed along with grain morphology and kernel average misorientations. This study will correlate the residual stress results with grain texture and KAM maps.

2. Methods

2.1. AM process

Gas atomized virgin Inconel 625 powder was procured from Carpenter Technologies with mean particle diameter size of 31.3 µm. A Concept Laser Mlab 100R commercial L-PBF system was used to fabricate Inconel 625 samples. The L-PBF system works with 100 W fiber laser at a wavelength of 70 nm. The samples were fabricated in an enclosed argon atmosphere to avoid any oxidation of alloy elements and provide unhampering flow of powder during the process. The elemental composition of virgin Inconel 625 powder used during L-PBF process was following the ASTM F3056-14 (21) standard. The elemental composition (in % wt) in the L-PBF powder and standard is presented in Table 1. 99.79% dense samples of dimension 10 mm^3 were fabricated using process parameters: power = 90 W, scan speed = 800 mm/s, laser diameter = 80 µm, layer thickness = 25 µm, and hatch spacing = 80 µm. Samples were built in the vertical and diagonal direction as shown in Fig. 1. An island scanning strategy with a checkerboard pattern consisting of 5 × 5 mm squares used to build samples is shown in Fig. 1(b). Each island consisted of scan tracks that alternated in opposite directions. Inconel 625 plate (152.4 x 152.4 x 4.76 mm^3) was procured from Metalmen, NY, USA. The plate was manufactured per specification AMS5599. Small 1 x 1 x 0.5 cm samples were sectioned from the plate using wire electrical discharge machining (EDM) and used as reference metal. The chemical composition of wrought IN625 is indicated in Table 1.

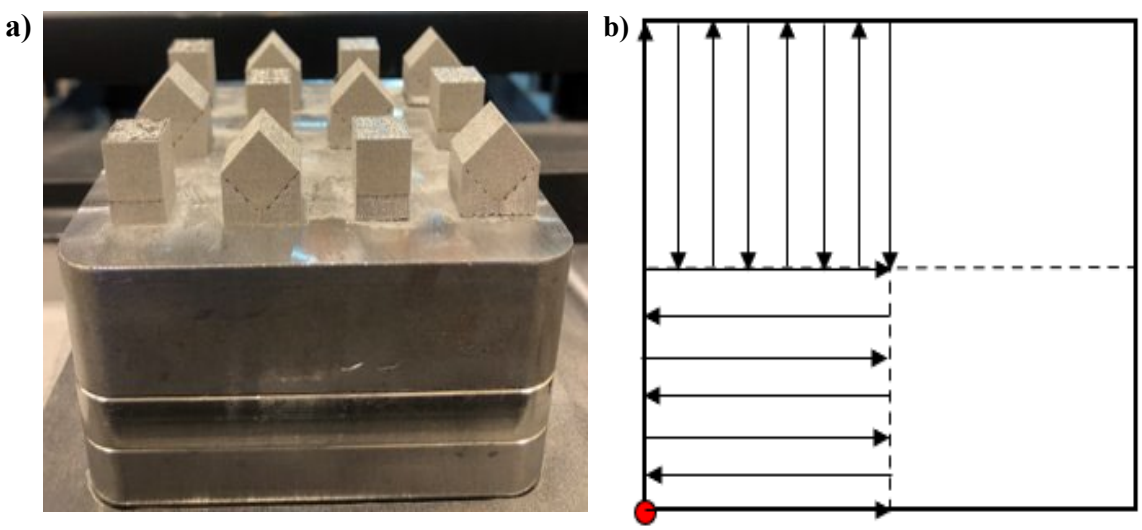

Figure 1: a) Inconel 625 samples built in vertical and diagonal orientations with support structures and b) island scan pattern with laser start point (red dot).

Table 1: Elemental composition as per ASTM standard, L-PBF powder, and wrought IN625 sample used in this study.

% wt.	Ni	Cr	Mo	Fe	Nb+Ta	Co	C	P	S	Al	Ti	Mn
ASTM	Bal	20-23	8-10	<5.0	3.15-4.15	<1	<0.1	<0.015	<0.015	<0.4	<0.4	<0.5
L-PBF	Bal	21.59	9.0	2.95	3.55	0.03	0.04	<0.015	<0.015	0.11	0.11	<0.5
Wrought	Bal	22.36	9.0	0.72	3.32	0.8	0.03	0.009	0.005	0.08	0.3	0.18

2.2. X-ray diffraction measurement

The XRD technique is the most widely used technique for measuring near surface residual stress as its penetration depth low – on-the-order of 10 µm. Herein, a portable Pulstec µ-X360 X-ray system was employed to carry out residual stress measurements. This system utilizes the novel Cos α method. The samples were irradiated using a beam current of 0.66 mA and voltage of 30 kV. The X-ray beam was directed to be incident on each sample at an angle of 28.8 degrees. The X-ray Manganese (Mn) *K*-alpha wavelength (λ) used for X-ray diffraction was 2.10 Å. The distance from the specimen and detector to capture the D-S ring image was set to D = 50 mm. The diffraction angle (2θ) was calculated using Bragg's law, i.e.:

$$n\lambda = 2d\sin\theta \tag{1}$$

where n is an integer and d is the d-spacing or interplanar spacing equal to 1.077 Å in this case. Using the above values, the diffraction angle was calculated as 155.03 degrees.

The µ-X360 X-ray Pulstec system utilizes the Cos α technique to calculate normal residual stress (σ_x) and shear residual stress (τ_{xy}) as presented in Fig 2(a). Keeping the angle of incident X-rays constant, the relative position of the D-S ring for the L-PBF parts (green ring) from that of the wrought part distortion D-S ring (black ring) was used to calculate strain as presented in Fig 2(b). In this study, the wrought ring position is considered stress free and the L-PBF ring is the stressed ring. The (311) family of crystallographic planes were used to create the D-S rings and for verifying the residual stress in as-built and heat-treated samples, as the (311) planes represent bulk macro stresses and are less sensitive to intergranular strain compared to other planes. Since a high level of tensile residual stress is generated at the top surface of the L-PBF samples due to the layer-wise AM process, the top oriented surface of each sample (surface facing upward during printing) was inspected. The equations used to calculate the in-plane stress and shear stress from strains are presented in Eqs. (2)-(5). The fundamental equations used to find the D-S ring radius and residual stress for this method are provided in more detail in [13][14].

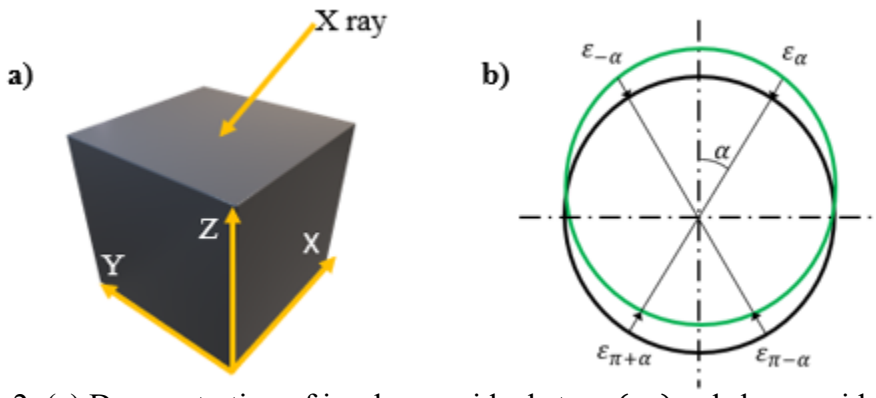

Figure 2: (a) Demonstration of in-plane residual stress(σ_x)and shear residual stress (τ_{xy}) direction on a sample surface and (b) schematic of D-S ring position of L-PBF samples (green ring) and wrought (black ring) Inconel 625 samples with four strains (ε) shown.

$$\varepsilon_{\alpha 1} = \frac{1}{2}\{(\varepsilon_{\alpha} - \varepsilon_{\pi+\alpha}) + (\varepsilon_{-\alpha} - \varepsilon_{\pi-\alpha})\} \quad (2)$$

$$\varepsilon_{\alpha 2} = \frac{1}{2}\{(\varepsilon_{\alpha} - \varepsilon_{\pi+\alpha}) - (\varepsilon_{-\alpha} - \varepsilon_{\pi-\alpha})\} \quad (3)$$

$$\sigma_x = -\frac{E}{1+v} \cdot \frac{1}{sin2\eta} \cdot \frac{1}{sin2\varphi_o} \cdot \left(\frac{\partial \varepsilon_{\alpha 1}}{\partial cos\alpha}\right) \quad (4)$$

$$\tau_{xy} = \frac{E}{2(1+v)} \cdot \frac{1}{sin2\eta} \cdot \frac{1}{sin\varphi_o} \cdot \left(\frac{\partial \varepsilon_{\alpha 2}}{\partial sin\alpha}\right) \quad (5)$$

where $\varepsilon_{\alpha 1}$ is the mean of the four principal strains, $\varepsilon_{\alpha 2}$ is the mean difference of the four principal strains as shown in Fig 1 (b), while $E = 214.58$ GPa and $v = 0.3$ are the Young's modulus and Poisson's ratio of Inconel 625, respectively.

2.3. EBSD analysis

Electron backscattered diffraction (EBSD) was used to study the effects of build orientation on grain orientation, texture, and kernel average misorientation. An analytical FEG-SEM FEI Nova Nano SEM 230 system was used in this study. Samples underwent standard grounding and polishing, followed by vibratory polishing for 2 hours. Similar procedures were performed on wrought IN625 samples to provide reference data. EBSD scans were performed on YZ sections of all samples. Inverse pole figure (IPF) and Kernel average misorientation (KAM) maps were captured in as built vertical, diagonal L-PBF and wrought IN625 samples to estimate local strain levels.

3. Results

3.1. Residual stress

Residual stress magnitudes and nature (tensile or compressive) were determined using the Cos α method along the top surface of the as-built vertically and diagonally printed L-PBF Inconel 625 samples as shown in Fig. 3. As seen from Fig. 3, the top surface of both as-built samples is dominated by tensile residual stress with a value of 77 ± 15 MPa and 52 ± 12 MPa, respectively. The vertically printed sample was found to possess higher detrimental tensile residual stress on its top surface compared to the diagonally printed sample surface. Similar results were concluded

from a study conducted by Pant et al. They measured maximum tensile residual stress in vertically printed IN718 samples [8]. This tensile residual stress is generated from the complex thermal gradients and rapid cooling rates (in the range of 10^3 K/s to 10^6 K/s) occurring during the L-PBF process. The intense solidification related to the high-power laser leaving the melt pool and freshly coated powder layers causes built layers under the exposed surface to contract. Peak tensile residual stress value is found in top layers of the built part. This is due to the cooling rate provided by the substrate is higher in the underlying layers of the sample. The high cooling rate is increased as the measured point move away from the substrate. Similar results were reported by Shuai et al. where they observed the formation of intense tensile residual stress in as-built L-PBF Inconel 625 samples [15]. In addition, vertically printed samples residual stress measurements had higher standard deviation compared to diagonally printed samples. This implies that the microstructure in the vertically printed sample was more anisotropic.

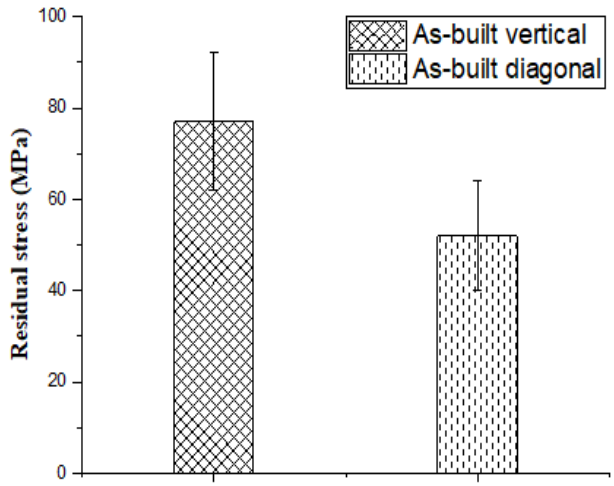

Figure 3: Residual stress measurement using Cos a method in vertically and diagonally printed L-PBF IN625 samples. Error bars represent standard deviation.

The D-S rings unique to Cos α method, used to calculate the strain values and ultimately residual stress values in vertically and diagonally printed samples are presented in Fig. 4. The D-S ring, which is recorded on a two-dimensional detector, is taken by the single exposure of X-rays, and this is an important working principle of the Cos α method. In Fig. 4., the cyan ring represents the D-S ring, and the green and yellow rings indicate inner and outer FWHM, respectively. As seen in Fig. 4, the ring distortion from the standard D-S ring position can be used to understand the nature and value of residual stress. The grey lines in Fig. 4 (lines appear as 'cross-hairs') indicate the position of a wrought Inconel 625 D-S ring position. Tensile residual stress within a sample shifts the D-S ring position below the grey lines. The presence of compressive residual stress moves the D-S ring position above the grey lines. As seen in Fig. 4., the D-S ring of the vertically built sample is further away from the top grey line compared to the D-S ring of the diagonally built sample. The circularity of the D-S ring recorded in the vertically printed sample is seen to be more distorted compared to the diagonally printed indicating more micro strain present in the microstructure.

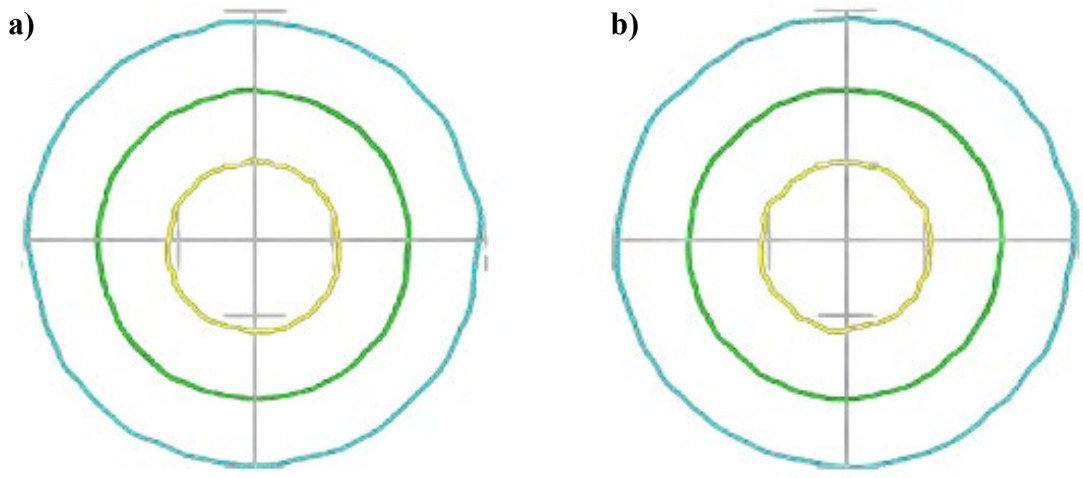

Figure 4: Debye-Scherrer ring distortion of (a) as-built vertically printed, (b) as-built diagonally printed L-PBF Inconel 625 samples. Cyan, green, and yellow rings indicate D-S ring position, inner and outer FWHM respectively.

3.2. EBSD

The difference in residual stress results presented in Fig. 3 can be better understood by performing EBSD to study the crystallography and morphology of grains. The EBSD results of L-PBF IN625 samples were compared with the wrought IN625 sample. Fig. 5 shows the IPF maps of the YZ cross-sections for the as built vertically, diagonally, and wrought samples. As seen in Fig. 5(a), as built sample exhibit texture, with grains oriented in Z- direction. The grains are elongated in Z-direction or build direction, which is inherited from the L-PBF process. A series of columnar grains growing through several layers of powder oriented parallel to the build direction was seen in Fig. 5(a). This is the consequence of directional heat transfer taking place during the solidification stage of printing process. The high cooling rate supplied by the build substrate to every new melted powder layer, helps to adhere with previously melted layer to form elongated grains. This observation is in line with the literatures, where elongated grains along the build direction was reported in L-PBF as built parts [16]. The grains in diagonally printed sample as seen in Fig. 5(b) were observed to arrange themselves at some angle with respect to build direction. The texture quality in both oriented samples were observed to be similar with minimal variations. The grain morphology in wrought Fig. 5(c) was observed to be equiaxed and oriented in random angles.

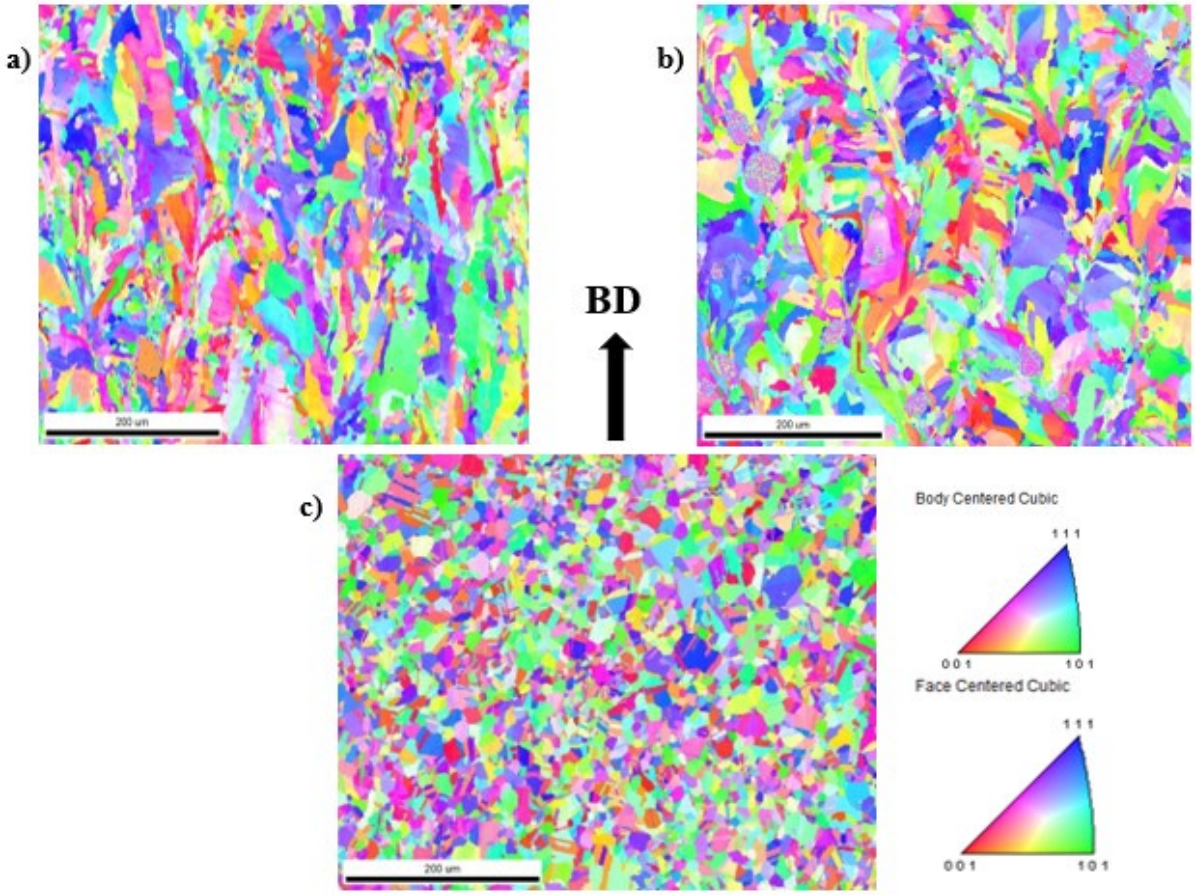

Figure 5: IPF of a) vertical as built, b) diagonal as built and c) wrought IN625 samples. BD stands for build direction. (Color crystalline orientation code is inserted)

The kernel average misorientation (KAM) maps presented in Fig. 6 for as built vertically and diagonally oriented, and wrought IN625 samples were used to further analyze the correlation between micro strain caused by dislocations in the microstructure. The KAM maps show the mean misorientation ratio of a given point and the mean orientation of its neighbors with the same grain. Regions with high KAM values commonly represent regions with plastic strain [17]. The scales enclosed in each KAM maps indicate the level of misorientations. The scales are very low in value which helps address the misorientations caused by dislocations in grains. The micro strain present in the microstructure is highlighted by the green regions. As seen in Fig. 6(a), the micro strain in the as-built vertically printed L-PBF sample is denser compared to diagonally printed sample. indicating presence of high residual stress. The presence of micro strain in the microstructure is coupled with the presence of high dislocation density which is inherited during the L-PBF process. Dislocations in diagonally built sample were less dense compared to vertically built IN625 sample in Fig. 3. This confirms the lower residual stress caused by local strain in diagonally printed sample observed in Fig.2. KAM map of wrought IN625 sample is presented in Fig. 6(c) as a benchmark data. The blue circular spots in L-PBF as built samples KAM maps indicate presence of pores arises during the L-PBF build process.

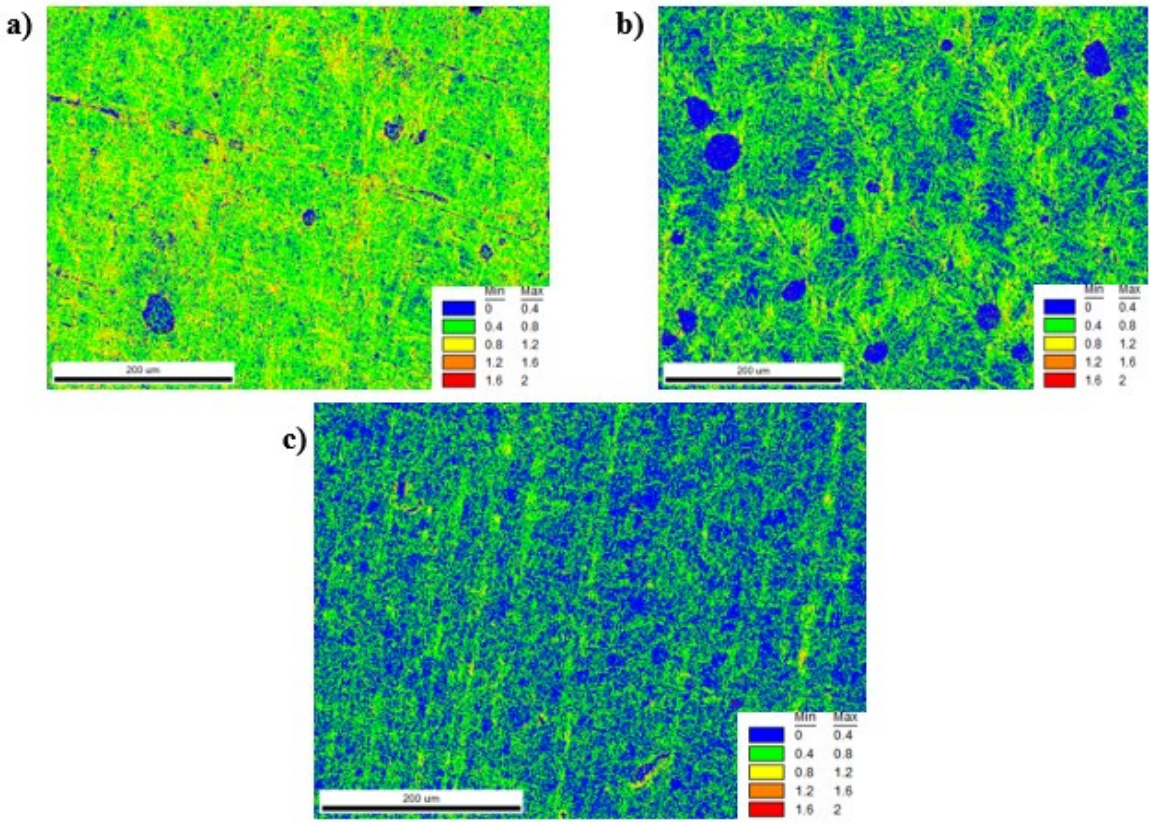

Figure 6: KAM maps for a) vertically as built, b) diagonally as built, and c) wrought IN625 showing minor misorientations caused by dislocations highlighted in green regions.

4. Conclusions

In this study, the effect of build orientation (vertical and diagonal) on residual stress and microstructure was investigated in L-PBF Inconel 625. A novel Cos α X-ray diffraction method was used to measure surface and sub-surface residual stress. The residual stress results were supported by microstructure analysis via EBSD. The major findings from this study are summarized below:

- With the same L-PBF system and process parameters, the vertically as built IN625 sample exhibited higher (77 ± 15 MPa) detrimental tensile residual stress compared to the diagonally printed sample (52 ± 12 MPa).
- The D-S ring captured using the Cos α method was found to be more distorted in the vertically built sample compared to the diagonally built. This is possibly from stressed grains which diffract the X-ray back to 2D detector in an unorderly path.
- The inverse pole figure results revealed minimal differences in grain morphology between two build orientations.
- Kernel average misorientation maps showed that the vertically printed sample inherited dense dislocations which precedes the formation of micro strain and residual stress.

The results presented and discussed in this study will enhance the understanding of the effect of build orientation on residual stress in directed energy additively manufactured parts. Residual

stress can inflict undesirable properties in parts applied in critical industry sectors such as aerospace, biomedical, nuclear, etc. This study can help designers/engineers understand how build orientation effects can be considered when designing and fabricating complex components.

Acknowledgement

This material is based upon work supported by the U.S. Department of Energy's Office of Nuclear Energy under Award Number DE-NE0008865.

Disclaimer

References

[1] ISO/ASTM, "INTERNATIONAL STANDARD ISO / ASTM 52900 Additive manufacturing — General principles — Terminology," *International Organization for Standardization*, vol. 5, no. I, pp. 1–26, 2015.

[2] P. Edwards and M. Ramulu, "Fatigue performance evaluation of selective laser melted Ti–6Al–4V," *Materials Science and Engineering: A*, vol. 598, pp. 327–337, 2014, doi: https://doi.org/10.1016/j.msea.2014.01.041.

[3] K. Mahesh, J. T. Philip, S. N. Joshi, and B. Kuriachen, "Machinability of Inconel 718: A critical review on the impact of cutting temperatures," *Materials and Manufacturing Processes*, vol. 36, no. 7, pp. 753–791, 2021, doi: 10.1080/10426914.2020.1843671.

[4] D. M. D'Addona, S. J. Raykar, and M. M. Narke, "High Speed Machining of Inconel 718: Tool Wear and Surface Roughness Analysis," *Procedia CIRP*, vol. 62, pp. 269–274, 2017, doi: 10.1016/j.procir.2017.03.004.

[5] F. J. Xu, Y. H. Lv, B. S. Xu, Y. X. Liu, F. Y. Shu, and P. He, "Effect of deposition strategy on the microstructure and mechanical properties of Inconel 625 superalloy fabricated by pulsed plasma arc deposition," *Materials & Design*, vol. 45, pp. 446–455, 2013, doi: https://doi.org/10.1016/j.matdes.2012.07.013.

[6] V. Shankar, K. Bhanu Sankara Rao, and S. L. Mannan, "Microstructure and mechanical properties of Inconel 625 superalloy," *Journal of Nuclear Materials*, vol. 288, no. 2, pp. 222–232, 2001, doi: https://doi.org/10.1016/S0022-3115(00)00723-6.

[7] G. R. Thellaputta, P. S. Chandra, and C. S. P. Rao, "Machinability of Nickel Based

Superalloys: A Review," *Materials Today: Proceedings*, vol. 4, no. 2, pp. 3712–3721, 2017, doi: 10.1016/j.matpr.2017.02.266.

[8] P. Pant *et al.*, "Mapping of residual stresses in as-built Inconel 718 fabricated by laser powder bed fusion: A neutron diffraction study of build orientation influence on residual stresses," *Additive Manufacturing*, vol. 36, no. February, p. 101501, 2020, doi: 10.1016/j.addma.2020.101501.

[9] P. Mercelis and J. P. Kruth, "Residual stresses in selective laser sintering and selective laser melting," *Rapid Prototyping Journal*, vol. 12, no. 5, pp. 254–265, 2006, doi: 10.1108/13552540610707013.

[10] J.-P. Kruth, J. Deckers, E. Yasa, and R. Wauthlé, "Assessing and comparing influencing factors of residual stresses in selective laser melting using a novel analysis method," *Proceedings of the Institution of Mechanical Engineers, Part B: Journal of Engineering Manufacture*, vol. 226, no. 6, pp. 980–991, 2012, doi: 10.1177/0954405412437085.

[11] L. Parry, I. A. Ashcroft, and R. D. Wildman, "Understanding the effect of laser scan strategy on residual stress in selective laser melting through thermo-mechanical simulation," *Additive Manufacturing*, vol. 12, pp. 1–15, 2016, doi: 10.1016/j.addma.2016.05.014.

[12] J. GUO, H. FU, B. PAN, and R. KANG, "Recent progress of residual stress measurement methods: A review," *Chinese Journal of Aeronautics*, vol. 34, no. 2, pp. 54–78, 2021, doi: 10.1016/j.cja.2019.10.010.

[13] K. Tanaka, "The cosα method for X-ray residual stress measurement using two-dimensional detector," *Mechanical Engineering Reviews*, vol. 6, no. 1, pp. 18-00378-18–00378, 2019, doi: 10.1299/mer.18-00378.

[14] T. Sasaki, Y. Hirose, K. Sasaki, and S. Yasukawa, "Influence of image processing conditions of Debye Scherrer ring images in X-ray stress measurement using an imaging plate ," *JCPDS-International Centre for Diffraction Data*, no. C, 1997.

[15] L. Shuai, Q. Wei, Y. Shi, J. Zhang, and L. Wei, "Micro-crack formation and controlling of Inconel625 parts fabricated by selective laser melting," *Solid Freeform Fabrication 2016: Proceedings of the 27th Annual International Solid Freeform Fabrication Symposium - An Additive Manufacturing Conference, SFF 2016*, pp. 520–529, 2016.

[16] T. De Terris, O. Castelnau, Z. Hadjem-hamouche, H. Haddadi, V. Michel, and P. Peyre, "Analysis of As-Built Microstructures and Recrystallization Phenomena on Inconel 625 Alloy Obtained via Laser Powder Bed Fusion (L-PBF)," *Metals*, vol. 11, no. 4, p. 619, 2021, [Online]. Available: https://doi.org/10.3390/met11040619.

[17] A. S. Gill, A. Telang, C. Ye, S. R. Mannava, D. Qian, and V. K. Vasudevan, "Localized plastic deformation and hardening in laser shock peened Inconel alloy 718SPF," *Materials Characterization*, vol. 142, no. May, pp. 15–26, 2018, doi: 10.1016/j.matchar.2018.05.010.